Rochester Institute of Technology

RIT Scholar Works

1-1-2018

Measurements of Radiation Pressure Owing to the Grating Momentum

Ying-Ju Lucy Chu
Rochester Institute of Technology

Eric M. Jansson
Charter School of Wilmington

Grover A. Swartzlander

Recommended Citation

Measurements of Radiation Pressure Owing to the Grating Momentum

Ying-Ju Lucy Chu,[1] Eric M. Jansson,[2] and Grover A. Swartzlander, Jr.[1,*]

[1]*Chester F. Carlson Center for Imaging Science, Rochester Institute of Technology, Rochester 14623, New York, USA*
[2]*Charter School of Wilmington, Wilmington 19807, Delaware, USA*

The radiation pressure force on a nearly single-order diffraction grating was measured for a transmission grating near the Littrow angles at wavelengths of 808 and 447 nm. The component of force parallel to the grating agreed well with our prediction, being proportional to the product of the grating order and the ratio of the wavelength and grating period. The normal component of force varied with the incident angle, vanishing near the Littrow angle as expected. The measurements verify a correspondence between the Fourier grating momentum and the mechanical momentum. This Letter provides opportunities for in-space fly-by-light sailcraft as well as terrestrial applications.

Since Maxwell's first prediction in 1873 [1], radiation pressure has helped to describe phenomena ranging from the astronomical to the quantum realm. For example, the gravitational collapse of stars and accretion dynamics are governed by radiation pressure [2,3]. Experimental evidence of Kepler's 1619 explanation of comet tails [4,5] was later extended to the general distribution of interplanetary dust [6,7]. Terrestial applications have found uses in biology as optical tweezers [8], laser cooling of atoms [9,10], and macroscopic objects [11,12]. The detection of gravitational waves by means of laser interferometers requires an accounting of radiation pressure [13]. Microstructures such as optical wings [14] and slot waveguides have promising photonic applications [15,16]. Thin microfabricated sheets such as diffraction gratings and diffractive metamaterials [17–23] provide opportunities to marry recent developments in materials research with grand ambitions for in-space propulsion and navigation. For example, radiation pressure is one of the few methods of reaching distant stars with free sunlight [24,25] or extraordinarily powerful laser systems [26,27].

While plans for those sailcraft considered elementary attitude-controlled reflective sails, optical scientists have recently proposed passive or active diffractive sails that may provide superior control authority for near-Earth missions and beyond [28–30]. Unlike a reflective sail, which has only a normal component of force relative to the surface, a diffractive sail has both tangential and normal components of force. The latter is notable for changing sign, continuously passing through the zero-value point as the angle of incidence is varied. Moreover, the large tangential component of force of a diffractive sail may be particularly advantageous for raising or lowering the orbit of a sailcraft [28,30].

Although the magnitude of radiation pressure may seem relatively weak owing to its inverse relation to the speed of light, the force may be comparable to the gravitational force in outer space or in a quasineutrally buoyant liquid. The exertion of radiation pressure on a grating provides both astronautical opportunities to propel low-areal-density sailcraft through space and a new laboratory technique to assert noncontact forces in a liquid. Light-driven sails being developed for future space travel afford low-cost and inexhaustible energy for a myriad of missions [31–34]. Similar to the development of air flight in the early 1900s, sailcraft technology is likely to rapidly advance after in-space demonstrations reveal the extent of fly-by-light challenges. New materials and sailcraft architectures will be perfected to optimize particular mission objectives. For example, one may question whether a reflective film such as metal-coated polyester is the optimal means of transferring radiation pressure into a mechanical force or torque. As an alternative, a transmissive or reflective dielectric diffractive film may provide advantages related to efficiency, mass, heating, and attitude control. Electro-optics beam steering of a diffractive film [34] may be preferable to mechanical systems, especially if the sail area extends over hundreds of square meters.

In this Letter we examine the radiation pressure force on a fused silica transmission grating that has been optimized to diffract light mostly into one dominant order at the Littrow angle. To satisfy the law of conservation of momentum, the grating may be expected to react and move, owing to the redirected beam momentum. However, this prediction cannot be made with certainty for two reasons: First, radiation pressure on a diffraction grating has apparently never been measured. Second, light scattering from a structured surface may be complicated by multiple transmitted and reflected diffraction orders, as well as surface or guided waves that may randomly scatter from surface roughness, leak, or Bragg-scatter from the periodic structure [35–40]. Experimentation is therefore

needed to determine the magnitude of the force and to verify any theoretical model of the system.

The radiation pressure force on a nonabsorbing grating may be expressed as the mechanical reaction to optical diffraction (see S1 in the Supplemental Material [41]):

$$\vec{F} = (P_i/ck)\left(\vec{k}_i - \sum_m \eta_m \vec{k}_m\right), \tag{1}$$

where $\eta_m = P_m/P_i$ is the efficiency of the mth diffracted beam; P_i (P_m) is the incident (diffracted) beam power; energy conservation requires $\sum_m \eta_m = 1$; c is the speed of light; $\vec{k}_i$ ($\vec{k}_m$) is the incident (diffracted) wave vector, with $k = |\vec{k}_i| = |\vec{k}_m| = 2\pi/\lambda$; and λ is the wavelength of the beam of light. Absorptive heating of less than 0.02 (K) is expected for our fused silica grating [42] (see S2 in the Supplemental Material [41]), allowing us to ignore pressure from reradiation, convection, and outgassing. Given specific design and optical properties of the grating, the values of efficiency may be determined by numerical methods [23,35–39]. Alternatively, they may be experimentally determined as described below by measuring the power of the diffracted beams.

A simplified depiction of incident and diffracted beams for a single-diffraction-order grating, with corresponding angles θ_i, θ_t, and θ_r, is shown in Fig. 1. Phase-matching of the electromagnetic fields at the grating boundary provides a relation between the components of the wave vectors that are parallel to the surface:

$$(\vec{k}_i + m\vec{K}) \cdot \hat{p} = \vec{k}_m \cdot \hat{p}, \tag{2}$$

where $\vec{k}_m$ is the mth diffraction order (for either the reflected or transmitted beam), $\hat{p}$ ($\hat{n}$) is the unit vector

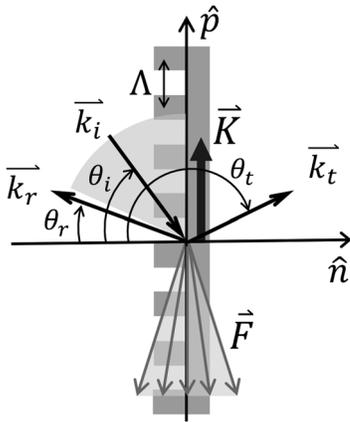FIG. 1. Plane of incidence for a diffraction grating of period Λ, with respective incident, reflected, and transmitted angles θ_i, θ_r, and θ_t; wave vectors $\vec{k}_i$, $\vec{k}_r$, and $\vec{k}_t$; and grating momentum $\vec{K} = (2\pi/\Lambda)\hat{p}$. For a single diffraction order, the force component parallel to the grating F_p is constant, whereas the normal component F_n may be positive, negative, or zero.

parallel (normal) to the grating surface, and $\vec{K} = (2\pi/\Lambda)\hat{p}$ is the fundamental wave vector associated with the grating period Λ; it is often called the grating momentum in Fourier optics (the scaling factor $\hbar$ is typically ignored). The well-known grating equation is a restatement of Eq. (2): $\sin \theta_m = -\sin \theta_i + m\lambda/\Lambda$. There is no transmitted diffracted beam when $\theta_m = \pm 90°$, which corresponds to a cut-off incidence angle $\theta_{i,c} = \sin^{-1}(m\lambda/\Lambda \mp 1)$. For example, the incident angle must exceed $\theta_{i,c} = 30°$ if $m = 1$, $\lambda = 808$ nm, and $\Lambda = 540$ nm.

For discussion purposes, let us first consider an ideal grating having unity transfer efficiency into a single diffraction order, allowing only an incident wave and either a transmitted or reflected wave. The parallel and normal force components of radiation pressure force may be expressed by the use of Eqs. (1) and (2), respectively:

$$F_p = -(P_i/c)(m\lambda/\Lambda), \tag{3a}$$

$$F_n = (P_i/c)(\cos \theta_i \pm [1 - \{m\lambda/\Lambda - \sin \theta_i\}^2]^{1/2}), \tag{3b}$$

where the minus (plus) sign is for a transmissive (reflective) diffraction order, and $\lambda/\Lambda = K/k_i$ is the ratio of the grating momentum and photon momentum. The parallel force $\vec{F}_p$ and $m\vec{K}$ are antiparallel as expected from conservation of momentum (e.g., see Fig. 1). That is, the value of $\vec{F}_p$ is directly related to the grating momentum $\vec{K}$. What is more, F_p is independent of the incident angle θ_i (assuming, of course, that the diffraction condition $|\theta_i| > |\theta_{i,c}|$ is satisfied). The normal component of force is positive below the Littrow diffraction angle, defined by the relation $2 \sin \theta_{i,L} = m\lambda/\Lambda$. For $|\theta_i| > |\theta_{i,L}|$, the normal component of force is negative, and the light source acts as a partial "tractor beam" [43–46]. At the Littrow angle, F_n vanishes.

In practice, a grating may diffract multiple orders, and the diffraction efficiency of each may vary with the incident angle and wavelength. In such cases, the expression of force must account for the momentum imparted by each grating order, which may be reflective or transmissive in nature (as indicated by the r and t subscripts below). If there is a dominant diffracted order, one may expect the force on the grating to be similar to the predictions described above. In general, the force components for a nonabsorbing grating may be expressed as

$$F_p = -\frac{P_i}{c}\sum_m [(\eta_{m,r} + \eta_{m,t})(m\lambda/\Lambda)], \tag{4a}$$

$$F_n = \frac{P_i}{c}\sum_m [\eta_{m,r}(\cos \theta_i + [1 - \{m\lambda/\Lambda - \sin \theta_i\}^2]^{1/2}) + \eta_{m,t}(\cos \theta_i - [1 - \{m\lambda/\Lambda - \sin \theta_i\}^2]^{1/2})], \tag{4b}$$

where $\eta_{m,r} = P_{m,r}/P_i$ and $\eta_{m,t} = P_{m,t}/P_i$ are the efficiencies of the mth-order diffracted beams at the wavelength λ,
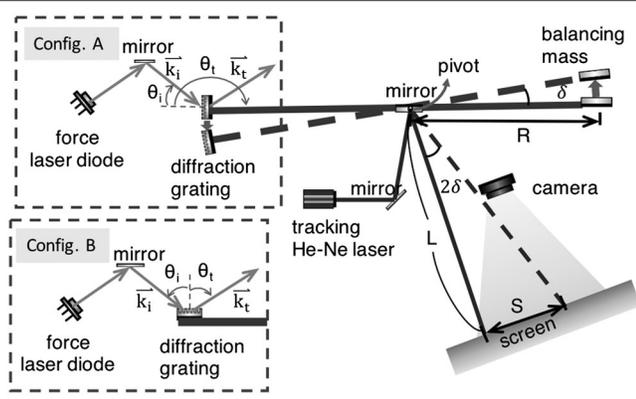
FIG. 2. Top view schematic. Torsion oscillator with moment arm of length R, angular displacement δ, forcing laser, tracking laser, camera, screen, and diffraction grating in configurations A and B.

TABLE I. Calculated Fresnel transmission coefficients $T(\theta_i)$ for a borosilicate bell jar with deduced grating scattering fraction $\eta_s = P_s/P_0$.

$\lambda = 808$ nm, $n = 1.51$	θ_i	30°	40°	50°	60°	
Configuration A	T_A	0.89	0.87	0.83	0.78	
Configuration B	T_B	0.78	0.83	0.87	0.89	
Scatter	η_s	0.17	0.19	0.13	0.23	

$\lambda = 447$ nm, $n = 1.53$	θ_i	15°	25°	35°	45°	55°	65°
Configuration A	T_A	0.9	0.9	0.88	0.85	0.8	0.74
Scatter	η_s	0.21	0.33	0.36	0.23	0.29	0.27

and $\sum_m (\eta_{m,r} + \eta_{m,t}) = 1$ owing to the conservation of energy. The values of efficiency are expected to change with incidence angle, and thus both components of force will vary with angle. A special case exists when the incident power is arbitrarily split between a transmitted and reflected beam, both of the same order, in which case Eqs. (3a) and (4a) agree, providing an angle-independent tangential force. We also note that like Eq. (3b), Eq. (4b) may in some cases allow a zero-valued normal force component at a particular incident angle, resulting in a purely tangential force.

Given the weak magnitude of the expected force $F \sim P_i/c < 5$ nN, we chose to measure the components of force within an evacuated bell jar by use of a custom-built torsion oscillator [47] as depicted in Fig. 2 (see S3 in the Supplemental Material [41]). We selected a commercially available single-order fused silica transmission grating having a period of $\Lambda = 540$ nm. The grating was attached to the torsion arm in one of two configurations: (A) with its surface normal parallel to the copper wire, or (B) with its surface normal perpendicular to the copper wire (see insets of Fig. 2). Separate experiments were performed with different lasers. The first laser ($\lambda = 808$ nm, $P_0 = 345$ mW) provided an efficient first-order diffraction at the Littrow angle. The second laser ($\lambda = 447$ nm, $P_0 = 1.5$ W) allowed both a first-order and a second-order Littrow angle. Weaker diffraction orders were also detected in both cases. The measured period of free oscillation of the torsion oscillator was $T_0 = 100.6$ s, and the characteristic decay time ($1/\alpha$) was roughly $80T_0$. Although the output power of the laser was constant, the power on the grating varied with incident angle owing to varied Fresnel transmission at the borosilicate bell jar surfaces. To account for this variability, we calculated the transmission through the bell jar, $T_A(\theta_i)$ and $T_B(\theta_i)$, for both configurations (see Table I) and determined the expected power at the grating, e.g., $P_i(\theta_i) = T(\theta_i)P_0$.

The diffraction grating was first mounted with its surface normal oriented parallel to the torsion arm, as depicted in Fig. 2, configuration A. The grating lines were transverse to the plane of incidence. With the bell jar removed, the oscillator was immobilized to allow measurements of the transmitted, diffracted, and reflected beams with the forcing laser ($\lambda = 808$ nm, and linear polarization transverse to the plane of incidence). The measured diffraction efficiencies and angles are depicted in Fig. 3(a) for four different angles of incidence between 30° and 60° (the incident wave vectors are shown without arrows). For this range, $\theta_i > \theta_{i,c}$, and the incident beam underfills the grating surface. The corresponding force components (described below) are shown in Fig. 3(b) as round black data points. The transmitted first-order diffraction efficiency was expected to be optimal near the Littrow angle $\theta_i = 48°$. In fact, both the 40° and 50° incident angles provided measured peak diffraction efficiencies of roughly 60%. The total measured diffracted power amounted to ~82% of the input beam power, suggesting that ~18% of the beam power was diffusely scattered (listed as $\eta_s = P_s/P_0$ in Table I). The scattering is attributed to power that does not diffract into allowed orders, but rather directly scatters or couples into guided waves and subsequently scatters [35–37,39,40].
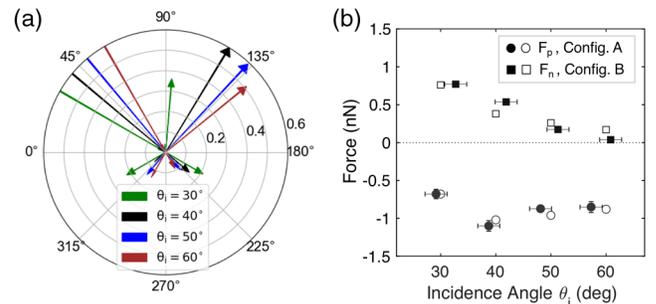

FIG. 3. Measured (a) diffraction efficiencies and angles, and (b) force components F_p and F_n, for $\lambda = 808$ nm, $P_0 = 345$ mW, and four angles of incidence. (a) The grating surface (not shown) is aligned along the 90°–270° line. (b) Torsion oscillator measurements (dark). Predicted values are based on efficiency measurements (white).
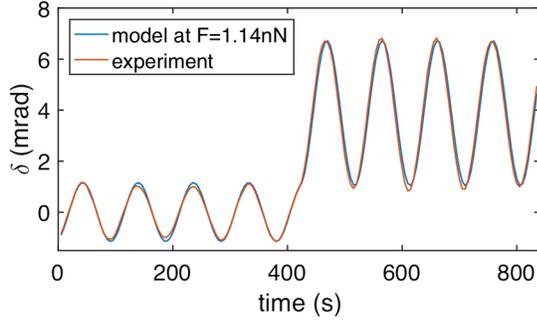
FIG. 4. Example of measured and modeled angular beam displacement: $\lambda = 808$ nm, $P_0 = 345$ mW, $\theta_i = 40°$. Fitted parameters: Shutter release time $t_0 = 420$ s, parallel force component magnitude $|F_p| = 1.14$ nN.

Next, we enclosed the oscillator within the bell jar, evacuated the chamber, and brought the free oscillator to a near standstill. The forcing laser power was set to $P_0 = 345$ mW, and a mechanical shutter was opened at time t_0 to provide a step-function force on the grating, resulting in an angular displacement such as that depicted in Fig. 4. This procedure was repeated three times for each of the four incidence angles described above. The time-varying angular displacement of the tracking laser upon the screen was extracted and fitted to the well-known equation for a weakly damped harmonic oscillator (see S4 in the Supplemental Material [41]), from which we derived force values for F_p. The excellent agreement between the experimental data and the oscillator model in Fig. 4 (typical RMS angular displacement error ∼0.08%) confirms both the veracity of the harmonic oscillator model and the high degree of mechanical stability and repeatability of our apparatus. The determined values of the tangential force F_p are plotted in Fig. 3(b), showing good agreement between the values of force that were measured with the torsion oscillator (dark circles with error bars) and the values predicted from the measured diffraction efficiencies using Eq. (4a) (white circles).

To obtain values of the normal component of force, we changed the orientation of the diffraction grating to configuration B (see Fig. 2) and recorded the laser-driven angular displacement of the torsion pendulum. The procedure described above was used to extract values of F_n, shown in Fig. 3(b) as dark squares with error bars. Again, we find relatively good agreement with the values predicted from Eq. (4b), shown as white squares in Fig. 3(b). As suggested above, the normal component of force is found to vanish, but unlike the case of a single-order grating where it vanishes at the Littrow angle, here we find $F_n = 0$ at $\theta_i \sim 60°$. Discrepancies between the measured values of force and the values predicted from efficiency measurements may be attributed to nonuniform scattering of the guided waves, which also assert radiation pressure.

To assess the radiation pressure at a wavelength that supports two Littrow angles, one at $\theta_i = 24°$ for $m = 1$ and
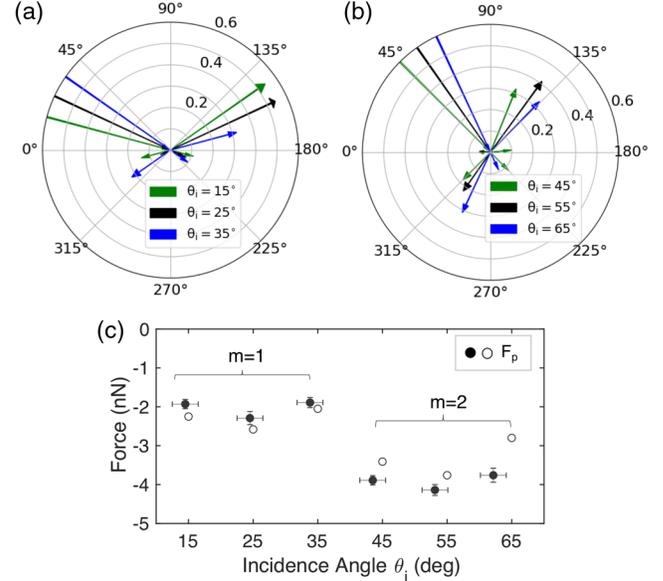

FIG. 5. Diffraction efficiencies and angles, and radiation pressure at $\lambda = 447$ nm, $P_0 = 1.5$ W. (a) $m = 1$ set: Measured efficiencies at incident angles θ_i near the first-order Littrow angle 24°. (b) $m = 2$ set: Same as (a), but near the second-order Littrow angle 56°. (c) Measured (black circles) and predicted (white circles) values of F_p.

another at 56° for $m = 2$, we substituted a laser having a wavelength $\lambda = 447$ nm and power $P_0 = 1.5$ W. If a single dominant diffraction order is produced at a given angle of incidence, we expect the value of F_p to scale with the value of m according to Eq. (3a). To verify this prediction, we mounted the grating in configuration A (see Fig. 2). The measured diffraction efficiencies of the transmitted and reflected beams are depicted in Fig. 5(a) for angles where there is a dominant first-order beam, and in Fig. 5(b) for angles where there is a dominant second-order beam (the incident wave vectors are shown without arrows). Values of force based on these efficiency values and Eq. (4a) are depicted as white circles in Fig. 5(c), whereas those obtained from the torsion oscillator are shown as black circles. Accounting for the angle-dependent transmission through the bell jar for the torsion oscillator experiments (see Table I), the average force efficiency, $\langle F_p c / T P_0 \rangle$, was 0.99 for the $m = 2$ set, and 0.46 for the $m = 1$ set, providing a ratio (2.15) that was 8% higher than the value (2.00) that would have been expected for a grating producing a single diffraction order (one near $\theta_i = 24°$, and the other near 56°). This agreement with the single-order approximation is remarkably good, supporting the direct relationship between the grating order m and F_p. Discrepancies were found between the measured forces and those predicted from the multiorder model [black and white circles in Fig. 5(c), respectively]. The differences, which are more pronounced than the 808 nm data, may be attributed to the wavelength-dependent scattering and wave

guiding. Scattering generally increases as the wavelength decreases. In fact, the scattered powers listed in Table I are greater at $\lambda = 447$ nm than at 808 nm.

In summary, we have used a vacuum torsion oscillator in two configurations at $\lambda = 808$ nm to measure the radiation pressure force both normal and parallel to a diffraction grating of period $\Lambda = 540$ nm. The grating produced a dominant transmitted diffraction order and a weaker transmitted and reflected order. The measured forces were qualitatively similar to those predicted for a grating producing a single diffractive order, and quantitatively in agreement with a multiorder model. The parallel component of force was relatively constant as the angle of incidence varied, whereas the normal component varied with angle, vanishing near the Littrow angle. An additional experiment at a shorter wavelength ($\lambda = 447$ nm) verified that the parallel component of radiation pressure force scales with the diffraction order, as expected when a single dominant order is diffracted. Experiments at both wavelengths confirmed that when there is a dominant diffraction order, the parallel component of force scales as the ratio of the optical wavelength and the grating period, λ/Λ—or equivalently, with the ratio of the grating momentum and wave momentum, K/k_i. That is, the so-called grating momentum, which is a construct from Fourier optics, has been verified to impart an equal and opposite mechanical momentum. Unlike a reflective surface that has only a normal component of radiation pressure force, a grating has been experimentally demonstrated to provide both normal and tangential components, thereby affording new optomechanical applications of diffractive films.

---

[*]Corresponding author: 54 Lomb Memorial Drive, Rochester, New York 14623, USA
gaspci@rit.edu

[1] J. C. Maxwell, *A Treatise on Electricity and Magnetism,* Vol. 1 (Clarendon Press, Oxford, England, 1881).
[2] K. Schwarzschild, Akad. Wissensch. Munchen, Sitz. **31,** 293 (1901).
[3] A. Eddington, Mon. Not. R. Astron. Soc. **79,** 2 (1918).
[4] P. Lebedev, Ann. Phys (Berlin) **6,** 433 (1901).
[5] E. Nichols and G. Hull, Astrophys. J. **17,** 352 (1903).
[6] L. Gindilis, N. Divari, and L. Reznova, Sov. Astron. **13,** 114 (1969).
[7] G. Schwehm, in *Interplanetary Dust and Zodiacal Light* (Springer, New York, 1976), pp. 459–463.
[8] A. Ashkin, Science **210,** 1081 (1980).
[9] P. D. Lett, R. N. Watts, C. I. Westbrook, W. D. Phillips, P. L. Gould, and H. J. Metcalf, Phys. Rev. Lett. **61,** 169 (1988).
[10] J. Dalibard and C. Cohen-Tannoudji, J. Opt. Soc. Am. B **6,** 2023 (1989).
[11] C. H. Metzger and K. Karrai, Nature (London) **432,** 1002 (2004).
[12] M. Bhattacharya, A. Vamivakas, and P. Barker, J. Opt. Soc. Am. B **34,** LO1 (2017).
[13] T. Corbitt, D. Ottaway, E. Innerhofer, J. Pelc, and N. Mavalvala, Phys. Rev. A **74,** 021802 (2006).
[14] G. A. Swartzlander, Jr., T. J. Peterson, A. B. Artusio-Glimpse, and A. D. Raisanen, Nat. Photonics **5,** 48 (2011).
[15] A. H. Yang, S. D. Moore, B. S. Schmidt, M. Klug, M. Lipson, and D. Erickson, Nature (London) **457,** 71 (2009).
[16] Q. Liu, X. Tu, K. W. Kim, J. S. Kee, Y. Shin, K. Han, Y.-J. Yoon, G.-Q. Lo, and M. K. Park, Sens. Actuators B **188,** 681 (2013).
[17] W. Stork, N. Streibl, H. Haidner, and P. Kipfer, Opt. Lett. **16,** 1921 (1991).
[18] C. Oh and M. J. Escuti, Opt. Lett. **33,** 2287 (2008).
[19] O. D. Lavrentovich, Proc. Natl. Acad. Sci. U.S.A. **108,** 5143 (2011).
[20] L. Marrucci, J. Nanophoton. **7,** 078598 (2013).
[21] Y. Zhang, L. Zhou, J.-Q. Li, Q.-J. Wang, and C.-P. Huang, Sci. Rep. **5,** 10119 (2015).
[22] N. V. Tabiryan, S. V. Serak, D. E. Roberts, D. M. Steeves, and B. R. Kimball, Opt. Express **23,** 25783 (2015).
[23] S. Gupta, J. Opt. Soc. Am. A **33,** 1641 (2016).
[24] R. H. Frisbee, Front. Propul. Sci. **227,** 31 (2009).
[25] P. Gilster, *Centauri Dreams: Imagining and Planning Interstellar Exploration* (Springer Science & Business Media, Berlin, 2004).
[26] G. Marx, Nature (London) **211,** 22 (1966).
[27] R. L. Forward, J. Spacecr. Rockets **21,** 187 (1984).
[28] G. A. Swartzlander, Jr., J. Opt. Soc. Am. B **34,** C25 (2017).
[29] K. Achouri and C. Caloz, arXiv:1710.02837.
[30] G. A. Swartzlander, Jr., arXiv:1805.05864 [J. Br. Interplanet. Soc. (to be published)].
[31] C. R. McInnes, *Solar Sailing: Technology, Dynamics and Mission Applications* (Springer Science & Business Media, Berlin, 2013), https://pdfs.semanticscholar.org/b58a/dc95f35af226872462eabd04f7c6a96e645d.pdf.
[32] C. Garner, B. Diedrich, and M. Leipold, NASA Technical Report No. JPC-99-2697, 1999, https://ntrs.nasa.gov/search.jsp?R=20000059207.
[33] L. Johnson, M. Whorton, A. Heaton, R. Pinson, G. Laue, and C. Adams, Acta Astronaut. **68,** 571 (2011).
[34] Y. Tsuda, O. Mori, R. Funase, H. Sawada, T. Yamamoto, T. Saiki, T. Endo, K. Yonekura, H. Hoshino, and J. Kawaguchi, Acta Astronaut. **82,** 183 (2013).
[35] D. L. Brundrett, E. N. Glytsis, and T. K. Gaylord, Opt. Lett. **23,** 700 (1998).
[36] T. Clausnitzer, T. Kämpfe, E.-B. Kley, A. Tünnermann, U. Peschel, A. Tishchenko, and O. Parriaux, Opt. Express **13,** 10448 (2005).
[37] P. Lalanne, J. P. Hugonin, and P. Chavel, J. Lightwave Technol. **24,** 2442 (2006).

[38] J. Francés, C. Neipp, S. Gallego, S. Bleda, A. Márquez, I. Pascual, and A. Beléndez, in *Optical Modelling and Design II*, Vol. 8429 (International Society for Optics and Photonics, Bellingham, WA, 2012), p. 84291U.

[39] A. V. Tishchenko and A. A. Shcherbakov, Opt. Express **25**, 13435 (2017).

[40] E. Bulgakov, D. Maksimov, P. Semina, and S. Skorobogatov, J. Opt. Soc. Am. B **35**, 1218 (2018).

[41] See the Supplemental Material at http://link.aps.org/supplemental/10.1103/PhysRevLett.121.063903 for S1. Radiation pressure force, S2. Laser heating and reradiated power, S3. Torsion pendulum construction parameters, and S4. Step-function response of a torsion pendulum.

[42] R. T. Swimm, Y. Xiao, and M. Bass, Appl. Opt. **24**, 322 (1985).

[43] A. Novitsky, C.-W. Qiu, and H. Wang, Phys. Rev. Lett. **107**, 203601 (2011).

[44] S. Sukhov and A. Dogariu, Phys. Rev. Lett. **107**, 203602 (2011).

[45] S. Sukhov and A. Dogariu, Opt. Lett. **35**, 3847 (2010).

[46] D. Palima, A. R. Bañas, G. Vizsnyiczai, L. Kelemen, T. Aabo, P. Ormos, and J. Glückstad, Opt. Express **21**, 581 (2013).

[47] G. Gillies and R. Ritter, Rev. Sci. Instrum. **64**, 283 (1993).

Measurements of Radiation Pressure owing to the Grating Momentum: Supplemental Material

Ying-Ju Lucy Chu[1], Eric M. Jansson[2], and Grover A. Swartzlander, Jr.[1*]

[1] *Chester F. Carlson Center for Imaging Science, Rochester Institute of Technology*
[2] *Charter School of Wilmington, Wilmington, Delaware*

S1. Radiation Pressure Force.

The momentum of a single photon of wavelength λ is given by the vector $\hbar \vec{k}$ where $k = 2\pi/\lambda$ is the magnitude of the wave vector, $c = \omega/k$ is the speed of light, and ω is the angular frequency. The energy of the photon is given by $E = \hbar\omega = \hbar c k$. A packet of N such photons passing through a plane over a time Δt carries a net momentum $N\hbar\vec{k}$. If the packet is elastically deflected by a material in another direction characterized by the wave vector $\vec{k}'$, the net momentum changes to $N\hbar\vec{k}'$. From Newton's third law, the force on the material is therefore

$$\vec{F} = \hbar N(\vec{k} - \vec{k}')/\Delta t = (P/ck)(\vec{k} - \vec{k}') \qquad \text{(S1)}$$

where $P = EN/\Delta t$ is the power of the beam of photons.

If instead the packet is elastically deflected in multiple directions, each characterized by a wave vector $\vec{k}_m$ and energy $N_m \hbar\omega$, where conservation of energy provides $\sum_m N_m = N$, then the above argument may be generalized:

$$\vec{F} = \hbar(N\vec{k} - \sum_m N_m \vec{k}_m)/\Delta t \qquad \text{(S2a)}$$

$$= (EN/ck)(\vec{k} - \sum_m (N_m/N)\vec{k}_m)/\Delta t \qquad \text{(S2b)}$$

$$= (P/ck)(\vec{k} - \sum_m \eta_m \vec{k}_m) \qquad \text{(S2c)}$$

where $\eta_m = N_m/N$ is the efficiency of scattering into the $\vec{k}_m$ direction. Conservation of energy and elastic scattering requires $\sum_m \eta_m = 1$ and the power of the mth beam is $P_m = N_m E/\Delta t = \eta_m P$.

S2. Laser heating and re-radiated power.

Assuming tabulated values for fused silica, e.g., $C_p = 750$ [J/kg-m] (specific heat) and $\rho = 2 \times 10^3$ [kg/m^3] (density), a beam of power $P = 1$ [W] and waist $w_0 = 5$ [mm], and a worst case value of the absorption coefficient in the near ultraviolet range, $\alpha_0 = 10^{-2}$ [m^{-1}] [1], the rate of heating is given by $d\tilde{T}/dt = I\alpha_0/\rho C_p$, where $I = 2P/\pi w_0^2$ for a Gaussian beam. We therefore calculate a worse case temperature rise of less than $\Delta\tilde{T} = 0.02$ [K] over a single oscillation period of 100.6 [s]. The re-radiated power owing to this temperature excess is found from the Stefan-Boltzmann law: $\Delta P = \sigma((\tilde{T} + \Delta\tilde{T})^4 - \tilde{T}^4)\pi w_0^2$, where $\sigma = 5.67 \times 10^{-8}$ [J·s·K^4/m^2] and $\tilde{T} = 300$ [K]. The re-radiated power, $\Delta P = 4.8 \times 10^{-4}$ [W] is significantly less that the incident power of 1 [W]. Laser heating may therefore be ignored in our experiment.

S3. Torsion pendulum construction parameters.

The torsion oscillator shown in FIG. 2 was constructed of a $D = 25$ [μm] diameter, $L_f = 240$ [mm] long tungsten filament (Alfa Aesar 10405-H4), and a $2R = 220$ [mm], $D' = 1$ [mm] diameter twist-hardened copper torsion arm. This system was attached to a grounded aluminum support frame. The diffraction grating and a balancing mass was attached to the two ends of the torsion arm. The commercially available grating (LightSmyth T-1850-800s-3210-93) was ground to a thickness of 190 [μm] to minimize the moment of inertia and thereby achieve large angular displacements. An aluminum balancing mass was placed on the other end of the copper torsion arm.

A small lightweight mirror was attached at the vertex of the torsion arm and filament to allow measurements of the angular displacement, $2\delta \approx S/L$, of a low power (less than 5 [mW]) HeNe tracking laser, where S is the linear displacement of the laser beam from its equilibrium position on a screen placed a distance $L = 1.92$ [m] from the pivot. Time lapse photographs (Canon 5D-III and Canon TC-80N3) of the screen were recorded at $\Delta t = 4$ [s] intervals. The position of the tracking beam was obtained by determining its centroid in each image.

The apparatus was placed on stand supported by a concrete-on-grade suburban basement floor that was remarkably free of vibrations and loading sag. A grounded aluminum wire mesh was shaped into a 300 [mm] high cylinder to serve as a Faraday cage, shielding the oscillator from inadvertent electrostatic torques. The system was centered within a customized borosilicate bell jar of good optical quality. After evacuating air from within the bell jar to a pressure of 10^{-5} [hPa] (7.5×10^{-6} [Torr]), the disturbed oscillator was brought to near rest by means of radiation pressure from the forcing laser. At this pressure the mean free path of the remaining air molecules exceeded the diameter of the bell jar. The system remained at rest for many hours – even while the vacuum system labored and people walked nearby.

Based on the calculated moment of inertia, $I = 1.0 \times 10^{-5}$ [kg·m^2], and the measured period, the torsional spring constant of the filament was determined to be $\kappa = (2\pi/T_0)^2 I = 3.9 \times 10^{-8}$ [N·m/rad]. This value agreed well with the theoretical value obtained from a tabulated value of the Young's modulus $Y = 410$ [kN·mm^{-2}] [2]: $\kappa' = \pi Y D^4/32L_f = 6.6 \times 10^{-8}$ [N·m/rad]. The discrepancy between the two values is attributed to the actual value of Y which depends on the working history of

the filament, and to the unknown variability of D along the length of the filament. We note that the radiation pressure force was not expected to induce significant linear pendular displacements of the total suspended mass $M = 2.4$ [g]. (In the worst case scenario with 5 [nN] applied to the deflection mirror rather than the grating, a linear pendulum would swing by only $FL_f/Mg \sim 50$ [nm].)

S4. Step function response of a torsion pendulum.
The equation of motion for angular displacement is

$$Id^2\delta/dt^2 + \gamma d\delta/dt + \kappa\delta(t) = FRu(t - t_0) \qquad \text{(S3)}$$

where $\gamma = 2I\alpha$ is a damping constant, $u(t - t_0)$ is a step function, and t_0 is the shutter release time. For small angular displacements, we assume the driving force, F is a constant. The solution of Eq. (S3) is found via Laplace transform techniques: $\delta(t) = \delta_1(t) + \delta_2(t)\, u(t - t_0)$ where

$$\delta_1(t) = \mathrm{e}^{-\alpha t}\, \delta_0\, \cos(\omega_1 t + \phi_0) + \frac{\mathrm{e}^{-\alpha t}}{\omega_1}\left(\frac{\alpha}{2}\,\delta_0 + \delta_0'\right) \quad \text{(S4)}$$

$$\delta_2(t) = \frac{F\,R}{\kappa}\left(1 - \mathrm{e}^{-\alpha\,(t - t_0)}\, \cos(\omega_1(t - t_0) + \phi_0)\right) \quad \text{(S5)}$$

and where $\delta_1(t)$ is the unforced solution of Eq. (S3) for $t < t_0$, $\delta_0 = \delta(t = 0)$, $\delta_0' = d\delta/dt\,|_{t=0}$, $\omega_0 = \sqrt{\kappa/I}$ is the natural oscillation frequency, $\omega_1 = \sqrt{\omega_0^2 - \alpha^2} = 2\pi/T_0 \approx \omega_0$ is the oscillation frequency, $T_0 = 100.6$ [s] is the measured oscillation period, $\alpha = 1/(80\,T_0)$ is the measured decay constant, and ϕ_0 is the initial phase at $t = 0$. Values of the unknown parameters are found by fitting δ_1 and δ_2 to the measured angular displacement data.

[1] R. T. Swimm, Y. Xiao, and M. Bass, Applied Optics **24**, 322 (1985).
[2] "Modulus of elasticity or young's modulus - and tensile modulus for common materials," "`http://www.engineeringtoolbox.com/young-modulus-d_417.html`", accessed on 2017-12-21.